

# VERTICAL BEAM SIZE MEASUREMENT AT CESR TA USING DIFFRACTION RADIATION

L. Bobb, JAI, Egham, Surrey, UK; DLS, Oxfordshire, UK

T. Aumeyr, P. Karataev, JAI, Egham, Surrey; Royal Holloway, University of London, Surrey, UK

E. Bravin, T. Lefevre, S. Mazzoni, H. Schmickler, CERN, Geneva, Switzerland

M. Billing, J. Conway, Cornell University, CLASSE, Ithaca, NY, USA

## Abstract

Over recent years the first Diffraction Radiation (DR) beam size monitor has been tested on a circular machine. At CEsrTA, Cornell University, USA, the sensitivity and limitations of the DR monitor for vertical beam size measurement has been investigated. DR emitted from 1 and 0.5 mm target apertures was observed at 400 and 600 nm wavelengths. In addition, interference between the DR signals emitted by the target and mask has been observed. In this report, we present the recent observations and discuss areas for improvement.

## INTRODUCTION

Diffraction Radiation (DR) describes photons which are emitted when a charged particle passes through a target aperture. In this case the charged particle does not intersect the boundary of the medium but interacts with the medium via its electric field. The field of the charged particle excites atomic electrons of the medium. Polarisation currents are produced which are accompanied by the emission of electromagnetic waves called diffraction radiation [1].

The DR spectral angular distribution can be calculated using Eq. 1 where the wave number is defined as  $k = 2\pi/\lambda$  and  $E_{x,y}$  are the polarisation components of the radiation integrated over the target surface. The total field of the radiation is dependent on the incident charged particle field [1,2].

$$\frac{d^2W}{d\omega d\Omega} = 4\pi^2 k^2 \left( |E_x|^2 + |E_y|^2 \right) \quad (1)$$

The far-field zone defined by the far-field condition in Eq. 2 where  $L$  is the distance from the target to detector,  $\gamma$  is the Lorentz factor and  $\lambda$  is the DR wavelength [3] is the region at which the angular distribution of DR is observed. The prewave zone is the region near the target where the far-field condition is not satisfied.

$$L \gg \frac{\gamma^2 \lambda}{2\pi} \quad (2)$$

As shown in Fig. 1, DR is emitted in two directions. Forward Diffraction Radiation (FDR) is emitted in the direction of the charged particle trajectory. Backward Diffraction Radiation (BDR) is emitted in the direction of specular reflection relative to the incident charged particle trajectory and the target tilt angle  $\theta_0$ . For high energy beams the emission of DR is considered to be non-invasive. The energy loss of the charged particles to DR is much less than the energy of

the fast moving charged particle. For this reason the particle velocity can be treated as constant to a good accuracy [1] and DR, particularly BDR, can be used for non-invasive beam diagnostics.

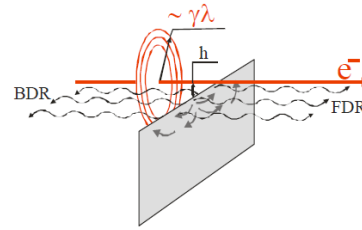


Figure 1: Schematic of DR emission from a particle moving in the vicinity of a medium where  $\gamma\lambda$  is the effective electric field radius and  $h$  is the impact parameter [2].

## EXPERIMENT SET-UP

The DR monitor is located in the L3 straight section of CEsrTA (see Fig. 2). The X-ray beam size monitor (xBSM) [5] located at the CHESS synchrotron radiation (SR) station is used to measure the vertical beam size  $\sigma_y$ . The visible beam size monitor (vBSM) [6] located in L3 approximately 10 m upstream of the DR target is used to measure the horizontal beam size  $\sigma_x$  [7, 8].

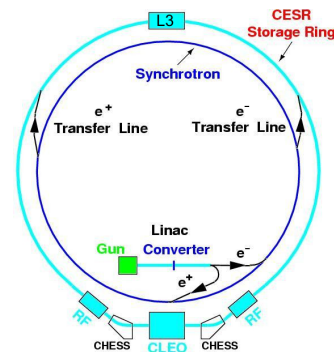


Figure 2: Layout of CEsrTA [4].

An overview of the DR tank is shown in Fig. 3. Inside the tank the target is attached to a mechanism with two degrees of freedom: translation IN/OUT and rotation about this axis. DR escapes from the DR tank via a viewport at the top which is connected to the optical system.

In Fig. 4 a schematic and photograph of the optical system are shown. The optical system is a dual purpose system providing direct imaging of the target surface using the achromat

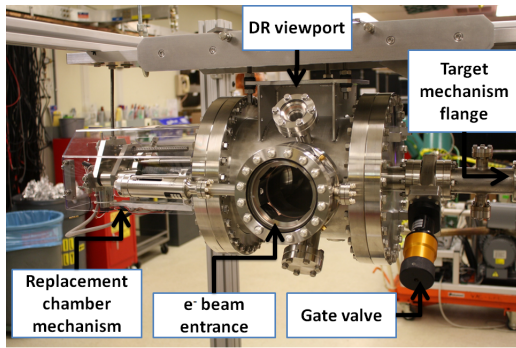


Figure 3: View of the DR target vacuum chamber from the upstream direction. The target is inserted from right to left.

and far-field imaging such that the angular distribution of DR can be observed using the planar convex (or biconvex) lens. In the latter case, since the compact optical system is within the prewave zone [3], the camera must be positioned at the back focal plane of the planar convex lens.

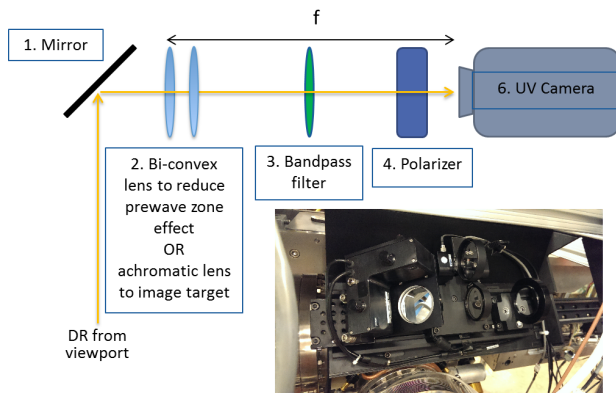


Figure 4: Schematic and image of the optical system.

Targets used on circular machines must be modified to have a fork-like shape since they must be retracted from the storage ring during injection and then inserted to the stored beam. The roughness, aperture size and coplanarity of the target must be controlled during fabrication to avoid distortions in the DR angular distribution.

Bonding by molecular adhesion is a technique that enables two substrates having polished surfaces to adhere to one another, without the application of adhesive [9]. The upper and lower tines of the target are machined separately in sets. The tines are then paired together in all variations to identify which upper/lower pairs result in the best coplanarity and attached to a flat mounting block. In effect, the molecular adhesion target consists of three individually machined pieces: two tines and the mounting block.

In this experiment a 0.5 mm molecular adhesion target made of Suprasil fused Silica ( $\text{SiO}_2$ ) glass with an Aluminium (Al) and Chromium (Cr) coating was used. This target was paired with a Silicon Carbide mask with 1 and 2 mm apertures. The mask was positioned 15.5 mm up-

stream of the target to reduce the synchrotron radiation (SR) background (see Fig. 5).

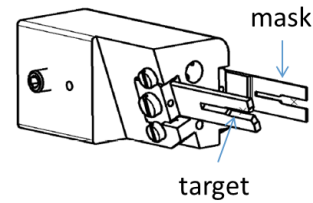


Figure 5: Schematic of the mask and target assembly.

## OPTICAL DIFFRACTION RADIATION (ODR) MODEL WITH PROJECTED VERTICAL POLARISATION COMPONENT (PVPC)

The author of [10] has shown that the vertical polarisation component is sensitive to beam size. It is assumed that electron beam has a Gaussian distribution [2].

In [11], the expression for the ODR vertical polarisation component convoluted with a Gaussian distribution is given and shown here in Eq. 3 where  $\alpha$  is the fine structure constant,  $\gamma$  is the Lorentz factor,  $\theta_0$  is the target tilt angle,  $t_{x,y} = \gamma\theta_{x,y}$  where  $\theta_{x,y}$  are the radiation angles measured from the mirror reflection direction,  $\lambda$  is the observation wavelength,  $\sigma_y$  is the rms vertical beam size,  $a$  is the target aperture size,  $\bar{a}_x$  is the offset of the beam centre with respect to the slit centre and  $\psi = \arctan \left[ \frac{t_y}{\sqrt{1+t_x^2}} \right]$ . This model is applicable when the TR contribution from the tails of the Gaussian distribution scraping the target is negligible i.e. approximately  $a \geq 4\sigma_y$ .

The projected vertical polarisation component (PVPC) takes the vertical (y) projection of the 3-dimensional ( $\theta_x$ ,  $\theta_y$ , intensity) DR angular distribution. The y-projection is obtained by integrating over the horizontal angle  $\theta_x$ . The visibility ( $I_{min}/I_{max}$ ) of the y-projection is sensitive to the beam size of the electron beam. The reader should refer to [11] for detailed steps to obtain the vertical beam size measurement.

## OPTICAL DIFFRACTION RADIATION INTERFERENCE (ODRI)

FDR produced by the mask interferes with BDR emitted by the target. Both of these DR sources will also interfere with background SR. The ODRI model uses Eq. 4 with parameters:

$$\begin{aligned}
 k &= \frac{2\pi}{\lambda} & f &= \sqrt{k_x^2 + \eta^2} \\
 k_x &= k \sin \theta \cos \phi & \beta &= \sqrt{1 - 1/\gamma^2} \\
 k_y &= k \sin \theta \sin \phi & \Phi_0 &= \frac{2\pi d}{\beta \lambda} (1 - \beta \cos \theta) \\
 \eta &= \frac{k}{\beta \gamma} & \Phi_1 &= \frac{2\pi \Delta}{\lambda}
 \end{aligned}$$

$$\frac{d^2 W_y^{slit}}{d\omega d\Omega} = \frac{\alpha\gamma^2 \exp\left(-\frac{2\pi a \sin \theta_0}{\gamma\lambda} \sqrt{1+t_x^2}\right)}{2\pi^2 \frac{1+t_x^2+t_y^2}{1+t_x^2}} \times \left\{ \exp\left[\frac{8\pi^2\sigma_y^2}{\lambda^2\gamma^2}(1+t_x^2)\right] \cosh\left[\frac{4\pi\bar{a}_x}{\gamma\lambda} \sqrt{1+t_x^2}\right] - \cos\left[\frac{2\pi a \sin \theta_0}{\gamma\lambda} t_y + 2\psi\right] \right\} \quad (3)$$

$$E_y = \frac{ie}{4\pi^2 c} \left\{ \left[ \frac{\exp[-(\frac{a_1}{2} + y - \delta)(f - ik_y)]}{f - ik_y} - \exp(i\Phi_1) \frac{\exp[-(\frac{a_1}{2} - y + \delta)(f + ik_y)]}{f + ik_y} \right] - \exp(i\Phi_0) \left[ \frac{\exp[-(\frac{a_2}{2} + y)(f - ik_y)]}{f - ik_y} - \exp(i\Phi_1) \frac{\exp[-(\frac{a_2}{2} - y)(f + ik_y)]}{f + ik_y} \right] \right\} \quad (4)$$

where  $\Delta$  is the coplanarity of the target tines in the longitudinal direction (i.e. along the trajectory of the electron),  $a_1$  is the mask aperture size,  $a_2$  is the target aperture size and  $d$  is the distance between the mask and target [12]. To observe the vertical angular distribution  $\phi = \pi/2$  and a suitable range of  $\theta$  is chosen. This model should be used when  $a_1 < 4a_2$ .

## BEAM SIZE SENSITIVITY

The xBSM was used as the reference beam size monitor from which we could compare the DR monitor measurements. A variety of beam sizes were measured at 600 nm wavelengths. From DR theory it is known that the sensitivity to beam size scales inversely with wavelength. However as aforementioned, at  $\lambda = 400$  nm the SR background was too high causing distortions to the DR angular distribution and inhibiting further analysis.

### ODR with PVPC Technique

In Fig. 6 the DR angular distribution in the case of negligible interference is shown. As expected, the central lobes have a greater intensity compared to the side fringes. In Fig. 7 the beam size sensitivity is demonstrated. The visibility of the vertical projections at 45  $\mu\text{m}$  beam size were larger than that at 17  $\mu\text{m}$  as expected. The 45  $\mu\text{m}$  line profile with a known beam offset relative to the target centre also had a greater visibility than that of the centred beam. Thus in Fig. 7 the ambiguity and contribution due to beam offset in the target aperture to the beam size measurement can be observed. The beam offset was observed from direct imaging of the target surface.

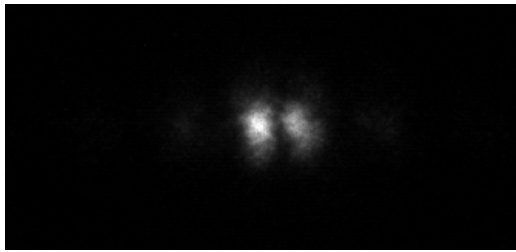


Figure 6: An example of the DR angular distribution:  $\lambda = 600$  nm, 0.5 mm target and 2 mm mask.

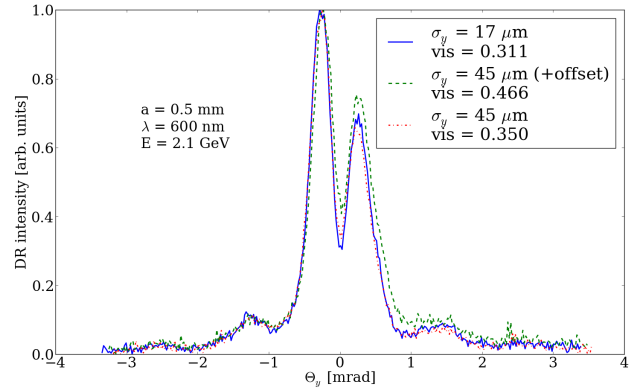


Figure 7: A comparison of projected vertical polarisation components (PVPCs) for different beam sizes.

Using the ODR model and PVPC technique, the expected visibility curves were simulated by obtaining the visibilities from simulated angular distributions using Eq. 3 for different beam sizes at 600 nm wavelength and 0.5 mm target. The simulated visibility curve assumes zero background thus the curve passes through the origin. The expected theoretical visibility curve was fitted to Eq. 5 [2] to obtain the coefficients  $A_{0,1,2}$ . The coefficient  $A_0$  defines the crossing point on the visibility axis. For real data measurements there will be some background contribution to the DR signal. Thus  $A_0$  will be larger than zero and this baseline represents the background contribution to beam size measurement.

$$R = A_0 + A_1\sigma_y + A_2\sigma_y^2 \quad (5)$$

Images at 17 and 45  $\mu\text{m}$  beam size and 600 nm wavelength were analysed. In Fig. 8 the measured visibility from each image was plotted (red crosses). The average visibility at each beam size was also plotted (green circles). From the simulated visibility curve the coefficients obtained were  $A_1 = -15.49$  and  $A_2 = 2.130 \times 10^7$ . Using the data and performing a least squares fit given  $A_1$  and  $A_2$ , the background offset for the real data was found to be  $A_0 = 0.292$ . This background offset was predominantly due to the SR.

As discussed, a significant SR contribution to the beam size measurement was observed at 600 nm wavelength. In

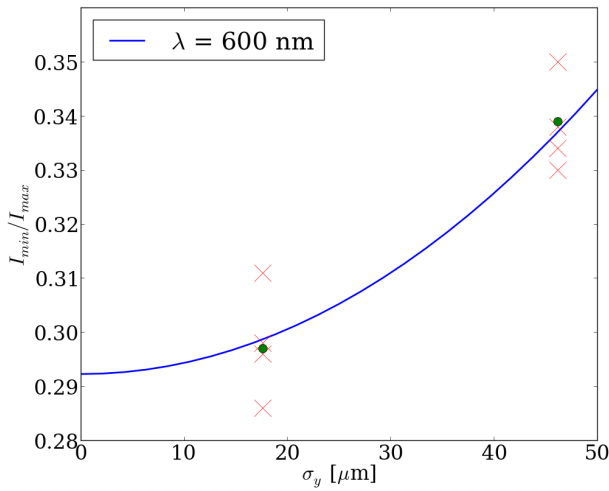


Figure 8: Resultant visibility curve at 600 nm wavelength and 0.5 mm target aperture from a least squares fit of the average visibility (green circles) at different beam sizes from individually measured visibilities (red crosses) corresponding to separate images.

this regime, it was found that SR contributed primarily as a background offset and did not modify the DR interference fringes noticeably. The beam size sensitivity improves with decreasing wavelength. However, in this experiment the SR contribution increased with decreasing wavelength. At 400 nm it was not possible to accurately measure the visibility due to the modification of the DR angular distribution due to SR. In Fig. 9 the distortion to the angular distribution at 400 nm in the 0.5 and 2.0 mm target and mask apertures respectively is shown.

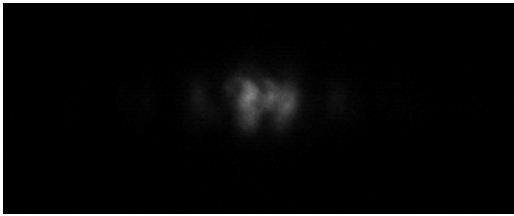


Figure 9: DR angular distribution at 400 nm wavelength and 0.5 mm target aperture.

### ODRI

In addition to beam size sensitivity, the ODRI model is also sensitive to the beam divergence. In the Monte Carlo application of the ODRI model, the summation of the DR intensity distribution for each electron of the beam is simulated. Therefore each electron is assigned a transverse position and divergence in the beam satisfying the user-defined beam profile. The beam profile and beam divergence are assumed to be Gaussian. To fit the beam size only, a reasonable estimate of the beam divergence was calculated. This was done by calculating the vertical beam emittance using the beam size measurement from the xBSM and the machine optics.

ISBN 978-3-95450-141-0

Table 1: Table of Beam Size and Divergence at the ODR Monitor

$\sigma_y(xBSM)$ [ $\mu\text{m}$ ]	$\varepsilon_y$ [m]	$\sigma_y(ODR)$ [ $\mu\text{m}$ ]	$\sigma'_y(ODR)$ [ $\mu\text{rad}$ ]
22.2	3.06E-11	17.6	4.08
46.1	1.70E-10	36.6	8.46
58.2	2.71E-10	46.2	10.7

The natural vertical emittance  $\varepsilon_y$  was calculated to be  $\sigma_y^2(xBSM)/\beta_y(xBSM) = 3.96 \times 10^{-11}$  m. From the vertical emittance the beam size and beam divergence were calculated as 17.6  $\mu\text{m}$  and 4.08  $\mu\text{rad}$  respectively. These results are summarised in Table 1.

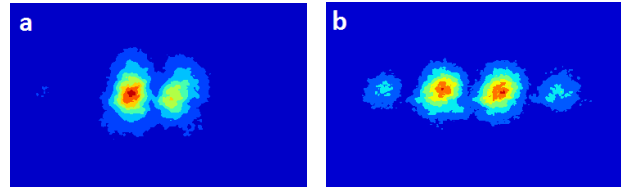


Figure 10: Contour plots of the angular distributions for a) ODR and b) ODRI.

In Fig. 10 the ODR and ODRI angular distributions may be compared. Fig. 10(a) shows the non-interference case (ODR) using a 0.5 mm target and 2.0 mm mask. Fig. 10(b) shows the interference case (ODRI) using a 0.5 mm target and 1.0 mm mask. As expected, an enhancement of the side fringes was observed due to the interference between FDR and BDR from the mask and target respectively.

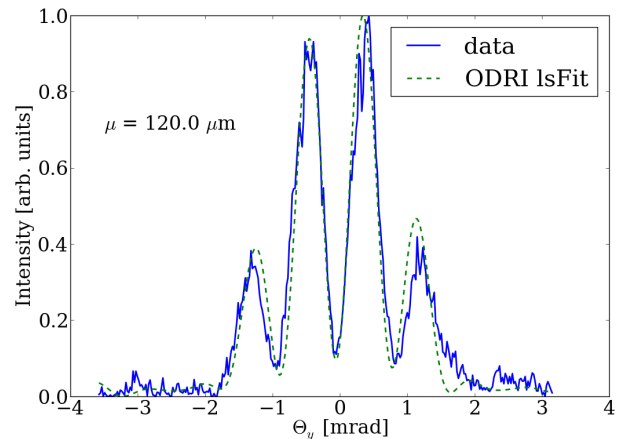


Figure 11: A beam offset of 120  $\mu\text{m}$  obtained using a least squares fit for ODRI data given parameters:  $\sigma_y = 17.6 \mu\text{m}$ ,  $\sigma'_y = 4.08 \mu\text{rad}$  and coplanarity offset 40 nm.

As aforementioned in addition to beam size, a beam offset relative to the centre of the target aperture also contributes to the visibility measurement. To quantify this beam position offset the line profile was fitted using the method of least squares. The result of the least squares fit is shown in Fig. 11.

Beam Profile Monitors

Monday poster session

The beam offset relative to the target aperture centre was found to be 120  $\mu\text{m}$ .

### SHADOWING OF THE ELECTROMAGNETIC FIELD

In the formation zone ( $L_f \approx \gamma^2 \lambda / 2\pi$ ) the Coulomb field of the ultra-relativistic ( $\gamma \gg 1$ ) electron and FDR from the aperture cannot be measured separately [13].

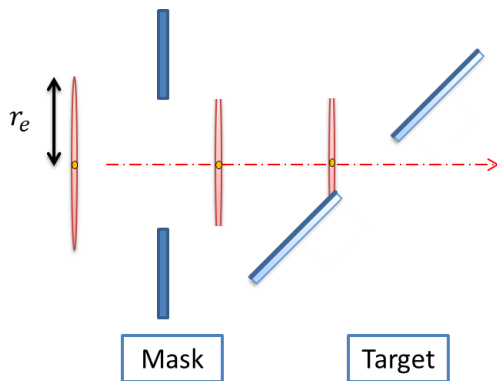


Figure 12: Shadowing of the Coulomb field of an electron passing through the mask and target.

In the Coulomb field point of view, the electric field associated with the electron beam is considered to consist of quasi-real photons. Scattering of the Coulomb field by the mask gives rise to FDR. Positioned downstream, the target is in the shadow of the mask (see Fig. 12). Thus it emits almost no radiation. The Coulomb field is gradually “repaired” during the formation zone [13].

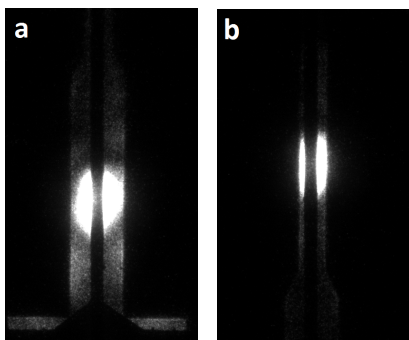


Figure 13: Images of the 0.5 mm target surface: (a) with negligible shadowing from a 2 mm mask and (b) with significant shadowing from a 1 mm mask where  $\lambda = 600 \text{ nm}$ .

In Fig. 13(a) negligible shadowing was observed and the measured radius of the illuminated DR disc in the vertical direction (perpendicular to the target edge) was 0.96 mm. The effective field radius for an electron  $r_e \approx \gamma \lambda / 2\pi$  given  $\gamma = 4110$  and  $\lambda = 600 \text{ nm}$  was 0.4 mm. A factor of two difference was obtained between the calculated and measured radii of illumination of the DR disc in the vertical direction.

Fig. 13(b) shows significant shadowing. The vertical width of the illuminated region has reduced from  $2 \times 0.96 =$

1.92 mm to 1 mm defined by the mask aperture. Here the reader should note the significance in this observation of clear evidence of the shadowing effect on the target surface. The mask is separated from the target and the optical system only images the target surface. Therefore although it is expected that SR cannot extend into the shaded regions of the target due to being blocked by the mask positioned upstream, DR emitted by the target should not have this boundary unless as a result of shadowing.

### CONCLUSION

In this paper vertical beam size measurements from the Diffraction Radiation monitor installed at CEsrTA are presented. Using a 0.5 mm target and 600 nm wavelength, interference effects in the angular distribution between the mask and target have been investigated. Further study of these interference effects have been explored via direct imaging of the target surface. These observations show evidence for the presence of shadowing.

### ACKNOWLEDGMENT

The author would like to thank the numerous colleagues who have participated in the project from CERN, Cornell University and Royal Holloway, University of London and the support of Diamond Light Source in presenting this research to the accelerator community.

## REFERENCES

- [1] A. P. Potylitsyn et al., *Diffraction Radiation from Relativistic Particles*, (Springer, Berlin Heidelberg, 2010)
- [2] P. Karataev, “Investigation of Optical Diffraction Radiation for Non-Invasive Low-Emittance Beam Size Diagnostics”, Thesis, 2004.
- [3] P. V. Karataev, “Pre-wave zone effect in transition and diffraction radiation: Problems and solutions”, *Physics Letters A*, 345 (2005) p. 428-438.
- [4] Cornell Electron Storage Ring, LEPP, Cornell University, <http://www.lepp.cornell.edu/Research/AP/CESR/>
- [5] N.T. Rider, et al., “Operation of a Single Pass, Bunch-by-Bunch X-ray Beam Size Monitor for the CESR Test Accelerator Research Program”, IBIC’12, Tsukuba, Japan, WECD01, p. 585.
- [6] S. Wang, et al., “A Turn-by-turn Beam Profile Monitor using Visible Synchrotron Radiation at CESR-TA”, IPAC’13, Shanghai, China, MOPWA073, p. 849.
- [7] L. Bobb et al., “UV/X-ray Diffraction Radiation for Non-intercepting Micron-scale Beam Size Measurement”, IBIC’12, Tsukuba, Japan, MOCC01, p. 24.
- [8] L. Bobb et al., “Diffraction Radiation Test at CEsR-TA for Non-Intercepting Micron-Scale Beam Size Measurement”, IBIC’13, Oxford, UK, WEAL3, p. 619.
- [9] S. Kerdiles, C. Duret, A. Vaufredaz and F. Metral, “Process for bonding by molecular adhesion”, Patent (2012), <http://www.google.com/patents/US8158013>
- [10] M. Castellano, “A new non-intercepting beam size diagnostics using diffraction radiation from a slit”, *Nucl. Instr. and Methods in Phys. Res. Sec. A: Accelerators, Spectrometers, Detectors and Associated Equipment*, 394, 3, (1997), p. 275-280.
- [11] P. Karataev, R. Hamatsu, T. Muto, S. Araki, H. Hayano, J. Urakawa, G. Naumenko, A. Potylitsyn and T. Hirose, “Application of optical diffraction radiation to a non-invasive low-emittance high-brightness beam diagnostics”, *QUANTUM ASPECTS OF BEAM PHYSICS. SINGAPORE : WORLD SCIENTIFIC PUBL CO PTE LTD*, (2004) p. 111-118
- [12] A. Cianchi, M. Castellano, L. Catani, E. Chiadroni, K. Honkavaara and G. Kube, “Nonintercepting electron beam size monitor using optical diffraction radiation interference”, *Phys. Rev. ST Accel. Beams*, 14, (2011), 10, p. 102803-102812.
- [13] G. Naumenko, X. Artru, A. Potylitsyn, Y. Popov, L. Sukhikh and M. Shevelev, “Shadowing of the electromagnetic field of relativistic charged particles”, *Journal of Physics: Conference Series*, 236, (2010), 1, p. 012004.